The 2009 IEEE/RSJ International Conference on
Intelligent Robots and Systems
October 11-15, 2009 St. Louis, USA

Dynamics and Control of an Omnidirectional Unmanned Ground Vehicle

Imad Khan and Matthew Spenko, *Member, IEEE*

Abstract— **An unmanned ground vehicle with the ability to change directions without a significant loss in speed would have superior mobility in confined spaces and tight corridors compared to Ackerman-steered or skid-steered vehicles. Omnidirectional vehicles, which can move in any planar direction regardless of their current kinematic pose, inherently have this capability. However, most omnidirectional vehicle designs are not practical for outdoor use because they are based on specialized wheels that can easily become clogged with dirt and debris. This paper presents a dynamic model of an omnidirectional UGV designed to operate in outdoor, real-world environments at speeds high enough to excite the dynamics of the vehicle. The analysis includes derivation of vehicle's equations of motion and a control strategy using inverse dynamics. Simulation results are shown to validate the model.**

I. Introduction

Unmanned Ground Vehicles (UGVs) are being used extensively in a variety of applications including military use, exploration, and disaster recovery [1], [2], [3]. In these applications, it is important that the UGVs maintain a high level of agility when operating in narrow passages, confined spaces, or cluttered environments. Agility is defined here as the ability to change direction without a significant loss in speed. This would allow a UGV to travel at a higher average speed, which will reduce its exposure to dangerous situations and allow it to complete its task in less time. The UGV will be better equipped to actively avoid hazards, especially those that are detected at close range.

The majority of UGVs being utilized in the field are either Ackermann or skid-steered [4], neither of which are inherently agile. However, an omnidirectional UGV—defined here as being capable of moving in any planar direction regardless of its current pose—is intrinsically agile, at least at low speeds. One of the goals of this project is to validate this claim for higher speeds. Most omnidirectional vehicles to date have been designed to operate on flat, clean, indoor surfaces. These vehicles usually utilize specialized wheels (e.g. [5], [6], [7]) that contain parts that can easily become clogged with dirt and debris. This prevents the designs from being implemented in outdoor environments.

This paper focuses on an omnidirectional vehicle design based on the Active Split Offset Caster (ASOC), first described in [8] (see Fig. 1). The ASOC is composed of two independently powered wheels that are "split" a distance L_S from each other and "offset" a distance L_O from an axis, α, that is free to rotate 360°. It can be shown that omnidirectionality can be achieved by connecting two or more ASOCs with rigid link at the α-axis [8], [9].

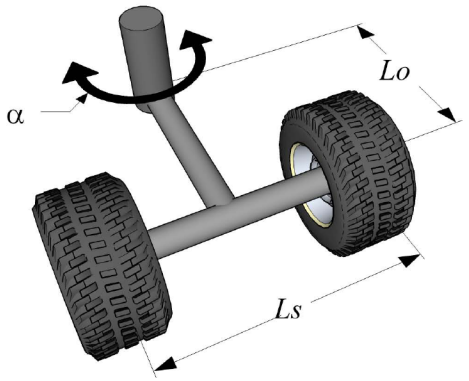

Fig. 1. Illustration of an Active Split Offset Caster (ASOC).

The design was chosen because it uses conventional wheels, can easily be coupled with classical suspension designs, has low scrubbing torque, and has a high kinematic isotropy value [10], [11], [12]. Conventional wheels make the UGV suitable for outdoor terrain and the suspension system allows it to operate on rough terrain and more easily traverse obstacles. Scrubbing torque is a measure of how much torque is lost as the wheels slip laterally during a turn, and the ASOC-based design has been shown to be superior to other designs in this regard [9]. Kinematic isotropy is defined as the condition in which a robot possesses a constant input/output velocity ratio for all possible output velocity directions [11]. It is essentially a measure of how close a robot is to a singular configuration. Ideally an omnidirectional robot should possess a kinematic isotropy measure of 1.0 for all joint configurations, which means that it would not have a preferred direction of travel. An ASOC-based omnidirectional UGV is more agile than other omnidirectional vehicles that use conventional wheels [13], [14]. For example, those robots are capable of moving sideways and rotating; however, they must stop and reorient their wheels before doing so, which means they have no inherent agility. Note that a high level of kinematic isotropy infers a high-level of agility, but the converse is not necessarily true—one could imagine a highly agile UGV that takes advantage of dynamic effects (e.g. controlled side slip) to gain agility.

This work was supported through startup funds provided by the Illinois Institute of Technology.

M. Spenko is on the Faculty of the Mechanical, Materials, and Aerospace Engineering Department, Illinois Institute of Technology, Chicago, IL 60616, USA. mspenko@iit.edu

Imad Khan completed his MS degree in the Mechanical, Materials, and Aerospace Engineering Department of Illinois Institute of Technology, Chicago. ikhan13@iit.edu

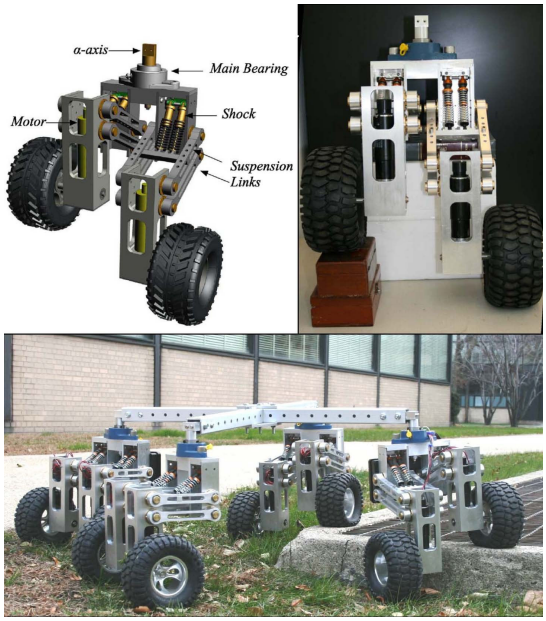

Fig. 2. CAD rendering and photograph of the prototype ASOC and the omnidirectional UGV comprised of four ASOCs. The distance between two opposing ASOCs is 84 cm.

The work presented here is based on the design of a man-portable omnidirectional UGV weighing approximately $30kg$ and capable of reaching $1.4m/s$ (see Fig. 2). With low vehicle mass and high speeds, vehicle control becomes more important than with previous implementations of the design. For example, a similar drive system was used on an assistive device that helped elderly people walk. It was assumed that the system was quasi-static, and thus only a kinematic controller that calculated wheel velocities based on the angular position of α was used [9], [15]. This paper details the derivation of the dynamic equations of motion for the system and compares an inverse dynamic controller with the previously implemented kinematic controller.

In Section II the dynamic equations of motion for this unique UGV are derived. Section III details the derivation of the controller and compares the results with the previously implemented kinematic controller.

II. Vehicle Dynamic Model

In this section the dynamic equations of motion for an omnidirectional UGV consisting of n ASOCs is presented. Note that only two ASOCs are required to achieve omnidirectional motion (with the addition of passive caster to maintain stability), but previous analysis has shown that three or four ASOCs are optimal when operating on terrain of various composition [11]. Fig. 3 shows a single ASOC in the inertial reference frame, and the complete UGV using n ASOCs is shown in Fig. 4. The nomenclature for the model is given in Table I. Note that the external forces acting on the wheels would need to be measured in real-time on an experimental system. Although challenging, estimation of these forces is not unprecedented [16], [17].

TABLE I

Nomenclature for the Dynamic Model

Symbol	Description
$\mathbf{I}$	Inertial reference frame
$\mathbf{C}$	Caster reference frame
L_O	Distance between C and wheel axle
L_S	Distance between wheels
r	Wheel radius
b	Distance between caster c.o.m and wheel axle
L	Distance of UGV c.o.m to caster axis
ω_i	Vector of right and left wheel angular velocities
$\mathbf{x}_i$	Position of i^{th} caster in $\mathbf{I}$, $\begin{bmatrix} x_i & y_i \end{bmatrix}$
α_i	Angular position of i^{th} caster w.r.t i_1 axis
$\dot{x}^C_{mi}$	Velocity of c.o.m of i^{th} caster along c_1
$\dot{y}^C_{mi}$	Velocity of c.o.m of i^{th} caster along c_2
$\mathbf{X}$	Position vector of UGV, $\begin{bmatrix} X & Y & \phi \end{bmatrix}$
ϕ	Angular position of UGV in $\mathbf{I}$
F^C_{ri}, F^C_{li}	Longitudinal forces from the wheels in $\mathbf{C}$
R^C_{ri}, R^C_{li}	Lateral forces from the wheels in $\mathbf{C}$
F^C_{xi}, F^C_{yi}	Forces acting on the axis of i^{th} caster in $\mathbf{C}$
J_C	Moment of inertia of caster about the vertical axis
j_W	Moment of inertia of wheel about wheel's rotational axis
J	Moment of inertia of UGV body about vertical axis
m	ASOC mass
m_u	UGV body mass
$\boldsymbol{\tau}_i$	Driving torque acting on i^{th} caster wheels
k	Transmission gear ratio

Using inverse kinematics, the angular velocities of the wheels are related to the velocity of point C by:

$$\boldsymbol{\omega}_i = \mathbf{A}_i \dot{\mathbf{x}}_i \tag{1}$$

where:

$$\mathbf{A}_i = \frac{1}{r}\begin{bmatrix} \cos\alpha_i - \frac{L_S}{2L_O}\sin\alpha_i & \sin\alpha_i + \frac{L_S}{2L_O}\cos\alpha_i \\ \cos\alpha_i + \frac{L_S}{2L_O}\sin\alpha_i & \sin\alpha_i - \frac{L_S}{2L_O}\cos\alpha_i \end{bmatrix}$$

The angular velocity of the ASOC is related to the wheel velocities by:

$$\dot{\alpha}_i = \frac{r}{L_S}\left(\omega_{ri} - \omega_{li}\right) \tag{2}$$

Let $\dot{\mathbf{x}}_c = \begin{bmatrix} \dot{\mathbf{x}}_1^T & .... & \dot{\mathbf{x}}_n^T \end{bmatrix}^T$. The velocities of casters can be related to the robot velocity, $\dot{\mathbf{X}} = \begin{bmatrix} \dot{X} & \dot{Y} & \dot{\phi} \end{bmatrix}^{\mathbf{T}}$ by:

$$\dot{\mathbf{x}}_c = \mathbf{G}\dot{\mathbf{X}} \tag{3}$$

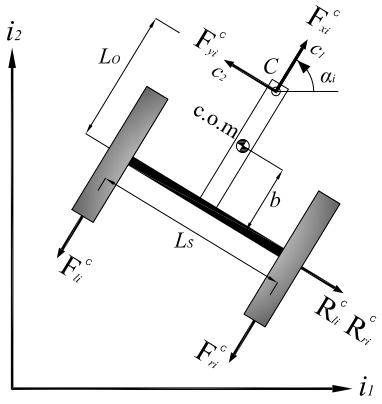

Fig. 3. An illustration of a single ASOC in the inertial reference frame. i_1 and i_2 are unit vectors in the X and Y directions.

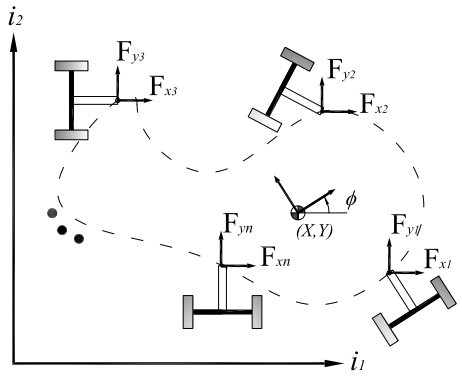

Fig. 4. Top view of the UGV model with arbitrary number of ASOCs.

where $\mathbf{G}$ is the associated Jacobian and can be computed as:

$$\mathrm{G} = \begin{bmatrix} \frac{\partial x_1}{\partial X} & \frac{\partial x_1}{\partial Y} & \frac{\partial x_1}{\partial \phi} \\ \frac{\partial y_1}{\partial X} & \frac{\partial y_1}{\partial Y} & \frac{\partial y_1}{\partial \phi} \\ \vdots & \vdots & \vdots \\ \frac{\partial x_n}{\partial X} & \frac{\partial x_n}{\partial Y} & \frac{\partial x_n}{\partial \phi} \\ \frac{\partial y_n}{\partial X} & \frac{\partial y_n}{\partial Y} & \frac{\partial y_n}{\partial \phi} \end{bmatrix}$$

Let the vector of wheel velocities be:

$$\boldsymbol{\omega} = \begin{bmatrix} \boldsymbol{\omega}_1^T & .... & \boldsymbol{\omega}_n^T \end{bmatrix}^T$$

and

$$\mathbf{A} = Diag\left(\mathbf{A}_1, ..., \mathbf{A}_n\right)$$

then $\boldsymbol{\omega}$ and $\dot{\mathbf{x}}_\mathbf{c}$ are related by:

$$\boldsymbol{\omega} = \mathbf{A}\dot{\mathbf{x}}_c \tag{4}$$

Thus,

$$\boldsymbol{\omega} = \mathbf{A}\mathbf{G}\dot{\mathbf{X}} \tag{5}$$

Balancing forces and moments acting on c.o.m of i^{th} caster give the following:

$$m\ddot{x}_{mi}^C = F_{ri}^C + F_{li}^C - F_{xi}^C \tag{6}$$

$$m\ddot{y}_{mi}^C = R_{ri}^C + R_{li}^C - F_{yi}^C \tag{7}$$

$$J_C\ddot{\alpha}_i + \left(R_{ri}^C + R_{li}^C\right)b + F_{yi}^C\left(L_O - b\right) = \left(F_{ri}^C - F_{li}^C\right)\frac{L_S}{2} \tag{8}$$

The non-holonomic no-slip constraint is given by the condition that the velocity of the point at the center of axle in the c_2 direction is zero. It is noted that this assumption may not hold in outdoor terrain consisting of loose, granular soil. This will be evaluated experimentally in future work. From this it can be shown that:

$$\dot{y}_{mi}^C = b\dot{\alpha}_i \tag{9}$$

Differentiating (9) and defining, $\mathbf{F}_i^C = \begin{bmatrix} F_{xi}^C & F_{yi}^C \end{bmatrix}^T$, $\dot{\mathbf{x}}_{mi}^C = \begin{bmatrix} \dot{x}_{mi}^C & \dot{\alpha}_i \end{bmatrix}^T$, and $\mathbf{F}_{Wi} = \begin{bmatrix} F_{ri}^C & F_{li}^C \end{bmatrix}^T$, then (6), (7), and (8) can be written as:

$$\mathbf{F}_{Wi} = \mathbf{B}_i\ddot{\mathbf{x}}_{mi}^C + \mathbf{D}_i\mathbf{F}_i^C \tag{10}$$

where:

$$\mathbf{B}_i = \frac{1}{2}\begin{bmatrix} m & \frac{2\left(J_C + mb^2\right)}{L_S} \\ m & \frac{-2\left(J_C + mb^2\right)}{L_S} \end{bmatrix}, \quad \mathbf{D}_i = \frac{1}{2}\begin{bmatrix} 1 & \frac{2L_O}{L_S} \\ 1 & \frac{-2L_O}{L_S} \end{bmatrix}$$

Using the transformation from $\mathbf{C}$ to $\mathbf{I}$, (10) can be written as:

$$\mathbf{F}_i = \mathbf{T}_{iC}^I\mathbf{D}_i^{-1}\left(\mathbf{F}_{Wi} - \mathbf{B}_i\ddot{\mathbf{x}}_{mi}^C\right) \tag{11}$$

where:

$$\mathbf{T}_{iC}^I = \begin{bmatrix} \cos\alpha_i & -\sin\alpha_i \\ \sin\alpha_i & \cos\alpha_i \end{bmatrix}$$

Thus the equation for the forces acting on the α axis of the i^{th} caster, we can map these forces on the UGV center using the Jacobian already given above. Let $\mathbf{F} = \begin{bmatrix} \mathbf{F}_1^T & .... & \mathbf{F}_n^T \end{bmatrix}^T$ and $\mathbf{M} = Diag\left(m_u, m_u, J\right)$ then forces and torques acting on the robot body can be given by:

$$\mathbf{M}\ddot{\mathbf{X}} = \mathbf{G}^T\mathbf{F} \tag{12}$$

$\mathbf{F}$ can be written as:

$$\mathbf{F} = \mathbf{D}^{-1}\left(\mathbf{F}_W - \mathbf{B}\ddot{\mathbf{x}}_m^C\right) \tag{13}$$

where:

$$\mathbf{D}^{-1} = Diag\left(\mathbf{T}_{1C}^I\mathbf{D}_1^{-1}, ..., \mathbf{T}_{nC}^I\mathbf{D}_n^{-1}\right)$$

$$\mathbf{B} = Diag\left(\mathbf{B}_1, ..., \mathbf{B}_n\right)$$

$$\mathbf{F}_W = \begin{bmatrix} F_{W1}^T & .... & F_{Wn}^T \end{bmatrix}^T$$

$$\ddot{\mathbf{x}}_m^C = \begin{bmatrix} \ddot{x}_{m_1}^{C^T} & \cdots & \ddot{x}_{m_n}^{C^T} \end{bmatrix}^T$$

The relation between the velocity of c.o.m of i^{th} caster in $\mathbf{C}$ and $\dot{\mathbf{x}}_i$ can be given as:

$$\dot{\mathbf{x}}_{mi}^C = \mathbf{E}_i\dot{\mathbf{x}}_i \tag{14}$$

where:

$$\mathbf{E}_i = \begin{bmatrix} \cos\alpha_i & \sin\alpha_i \\ -\frac{1}{L_O\sin\alpha_i} & \frac{1}{L_O\cos\alpha_i} \end{bmatrix}$$

Expanding (14) for all n ASOCs yields:

$$\dot{\mathbf{x}}_m^C = \mathbf{E}\dot{\mathbf{x}}_c \tag{15}$$

where:

$$\mathbf{E} = Diag\left(\mathbf{E}_1, ..., \mathbf{E}_n\right)$$

Using (3), (15) can be written as:

$$\dot{\mathbf{x}}_m^C = \mathbf{E}\mathbf{G}\dot{\mathbf{X}} \tag{16}$$

Differentiating (16) yields:

$$\ddot{\mathbf{x}}_m^C = \left(\dot{\mathbf{E}}\mathbf{G} + \mathbf{E}\dot{\mathbf{G}}\right)\dot{\mathbf{X}} + \mathbf{E}\mathbf{G}\ddot{\mathbf{X}} \tag{17}$$

Equation (17) gives the acceleration of the center of mass of the ASOCs. Now the wheel torques for each wheel are introduced assuming that the friction in the driving mechanism is negligible and defining:

$$\mathbf{R} = r\mathbf{I}_{2n} \tag{18}$$

$$\mathbf{K} = k\mathbf{I}_{2n} \tag{19}$$

$$\boldsymbol{\tau} = \begin{bmatrix} \boldsymbol{\tau}_1^T & .... & \boldsymbol{\tau}_n^T \end{bmatrix}^T \tag{20}$$

$$\mathbf{J}_W = j_W\mathbf{I}_{2n} \tag{21}$$

where $\mathbf{I}_{2n}$ is the $2n$ x $2n$ identity matrix. The actuator dynamics can be given as:

$$\mathbf{K}\tau = \mathbf{J}_W\dot{\omega} + \mathbf{R}\mathbf{F}_W \tag{22}$$

Differentiating (5) yields:

$$\dot{\omega} = \left(\dot{\mathbf{A}}\mathbf{G} + \mathbf{A}\dot{\mathbf{G}}\right)\dot{\mathbf{X}} + \mathbf{A}\mathbf{G}\ddot{\mathbf{X}} \tag{23}$$

Now using (12), (13), (17), (22), and (23) the direct dynamic model of the UGV can be written as:

$$\ddot{\mathbf{X}} = \mathbf{Y}\left(\mathbf{R}^{-1}\mathbf{K}\tau - \mathbf{Z}\dot{\mathbf{X}}\right) \tag{24}$$

where:

$$\mathbf{Y} = \left[\mathbf{M} + \mathbf{G}^T\mathbf{D}^{-1}\left(\mathbf{R}^{-1}\mathbf{J}_W\mathbf{A} + \mathbf{B}\mathbf{E}\right)\mathbf{G}\right]^{-1}\mathbf{G}^T\mathbf{D}^{-1} \tag{25}$$

$$\mathbf{Z} = \left(\mathbf{R}^{-1}\mathbf{J}_W\dot{\mathbf{A}} + \mathbf{B}\dot{\mathbf{E}}\right)\mathbf{G} + \left(\mathbf{R}^{-1}\mathbf{J}_W\mathbf{A} + \mathbf{B}\mathbf{E}\right)\dot{\mathbf{G}} \tag{26}$$

Equation (24) represents the equations of motion for a UGV employing n ASOCs. The procedure can easily be used to find equations of motion of a UGV with any number of ASOC modules.

III. Inverse Dynamic Control and Simulation

This section details a inverse dynamic control algorithm and compares the results to a kinematic controller used in previous work [9].

A. Inverse Dynamic Model

From (12) we can write:

$$\mathbf{F} = \mathbf{G}^{\#}\mathbf{M}\ddot{\mathbf{X}} \tag{27}$$

where $\mathbf{G}^{\#}$ is the right pseudo inverse of $\mathbf{G}$. Also from (13) we can write:

$$\mathbf{F}_W = \mathbf{D}\mathbf{F} + \mathbf{B}\ddot{\mathbf{x}}_m^C \tag{28}$$

Then using (17), (22), (23), (27), and (28) the inverse dynamic model can be written as:

$$\boldsymbol{\tau} = \mathbf{K}^{-1}\left(\mathbf{P}\dot{\mathbf{X}} + \mathbf{Q}\ddot{\mathbf{X}}\right) \tag{29}$$

where:

$$\mathbf{P} = \left(\mathbf{J}_W\dot{\mathbf{A}} + \mathbf{R}\mathbf{B}\dot{\mathbf{E}}\right)\mathbf{G} + \left(\mathbf{J}_W\mathbf{A} + \mathbf{R}\mathbf{B}\mathbf{E}\right)\dot{\mathbf{G}} \tag{30}$$

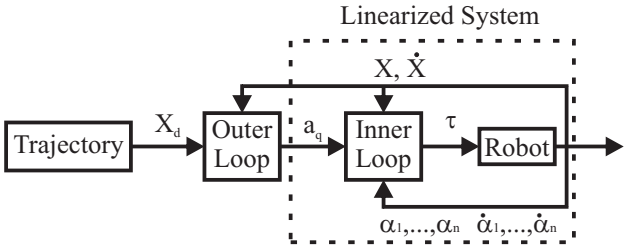

Fig. 5. Control architecture for the inverse dynamic model.

$$\mathbf{Q} = \mathbf{R}\mathbf{D}\mathbf{G}^{\#}\mathbf{M} + \left(\mathbf{J}_W\mathbf{A} + \mathbf{R}\mathbf{B}\mathbf{E}\right)\mathbf{G} \tag{31}$$

If the control input τ is chosen according to:

$$\boldsymbol{\tau} = \mathbf{K}^{-1}\left(\mathbf{P}\dot{\mathbf{X}} + \mathbf{Q}\mathbf{a}_\mathbf{q}\right) \tag{32}$$

then, the combined system of (29) and (32) will reduce to:

$$\ddot{X} = a_q \tag{33}$$

Setting $\mathbf{a_q}$ to:

$$\mathbf{a}_q = \ddot{\mathbf{X}}_d - \mathbf{K}_D\dot{\mathbf{e}} - \mathbf{K}_P\mathbf{e} \tag{34}$$

In (34) $\ddot{\mathbf{X}}_\mathbf{d}$ is the desired acceleration, $\mathbf{e}$ and $\dot{\mathbf{e}}$ are the errors in position and velocity respectively, and $\mathbf{K_P}$ and $\mathbf{K_D}$ are the proportional and derivative gains. Substituting (34) in (33) gives:

$$\ddot{\mathbf{e}} + \mathbf{K}_D\dot{\mathbf{e}} + \mathbf{K}_P\mathbf{e} = 0 \tag{35}$$

Equation (35) represents the inverse dynamics control law and provides the feedback linearization for trajectory tracking of UGV.

B. Simulation Results

The prototype vehicle has four ASOC modules as shown in Fig. 2. The Jacobian, $\mathbf{G}$, for the prototype vehicle with four equally spaced ASOCs can be given as:

$$\mathbf{G} = \begin{bmatrix} 1 & 0 & -L\sin\phi \\ 0 & 1 & L\sin\phi \\ 1 & 0 & -L\cos\phi \\ 0 & 1 & -L\sin\phi \\ 1 & 0 & L\sin\phi \\ 0 & 1 & -L\cos\phi \\ 1 & 0 & L\cos\phi \\ 0 & 1 & L\sin\phi \end{bmatrix}$$

On the experimental system, the angular position of the ASOC modules can be directly measured. For the simulation, angular positions and velocities are calculated using (2) and (5). Table II shows the physical parameters used for the simulation, which are based on the experimental system described earlier and control parameters that were tuned to yield suitable results.

Fig. 6 shows the desired trajectory of UGV in the XY plane, the trajectory of the UGV using the inverse dynamics controller, and the trajectory of the UGV using the kinematic controller.

TABLE II

PHYSICAL PROPERTIES USED IN THE SIMULATION

Parameter	Value	Units
m_u	1.98	kg
m	7.56	kg
j_W	0.0027	$kg \cdot m^2$
J_c	0.1577	$kg \cdot m^2$
J	0.1450	$kg \cdot m^2$
b	0.051	m
L_S	0.285	m
L_O	0.1425	m
r	0.08	m
L	0.415	m
k	1	—
$\mathbf{K}_P$	3	—
$\mathbf{K}_D$	1	—

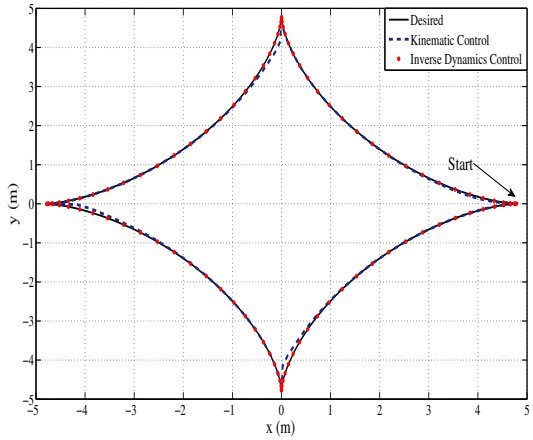

Fig. 6. Path tracking results comparing the inverse dynamics controller with a kinematic controller

Fig. 7 displays the total path tracking error of the UGV as a function of time when using the inverse dynamics controller and kinematic controller. The results indicate that the inverse dynamics controller performs significantly better than the kinematic controller. The RMS error for the inverse dynamics controller was 1.3 mm. For the kinematic controller the error was 21.7 mm. The differences are especially evident when the trajectory is discontinuous as a function of the path length.

A second trajectory is shown in Fig. 8 for the UGV. This trajectory was chosen to demonstrate the omnidirectional capabilities of the UGV. The desired orientation of the UGV was 0 $degrees$ throughout the path. Fig. 9 shows the orientation of the UGV in time for the tracked trajectory. Note that the UGV maintains its orientation for the entire path with negligible error for both inverse dynamics and kinematic controller. Fig. 10 shows the absolute velocity of the UGV for the step trajectory. For the inverse dynamics control the RMS absolute velocity of the UGV for the path is 3.21 m/sec, and for the kinematic control, the RMS absolute velocity is 3.20 m/sec. The elapsed time to regain the desired velocity at the edges was 1.0 $secs$ both the controllers. At the edges, the magnitude of the velocity does

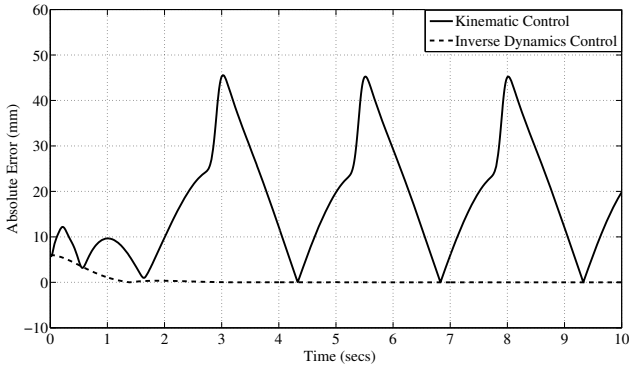

Fig. 7. Path tracking error against in time.

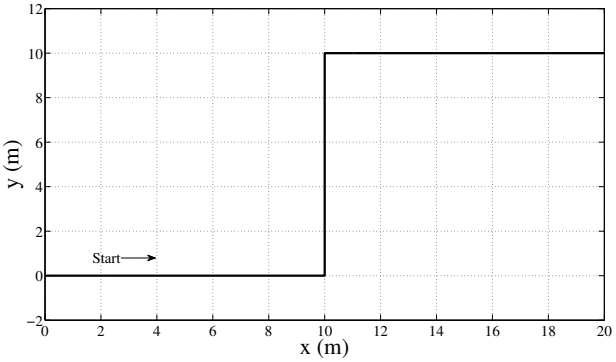

Fig. 8. Step trajectory for the simulation.

not fall below then 44.0% of the desired magnitude of 3 m/sec for the inverse dynamics control and approaches zero for the kinematic control. Fig. 11 shows the angular position of one ASOC in time. The ASOCs rotates by $\pi/2$ $radians$ at the edges in approximately 0.5 s for both controllers.

IV. CONCLUSION AND FUTURE WORK

In this paper, the dynamic equations of motion for a unique omnidirectional UGV consisting of an arbitrary number of ASOCs were derived and an inverse dynamics based controller was chosen to analyze the model. Using simulations an inverse dynamics control law was compared to a

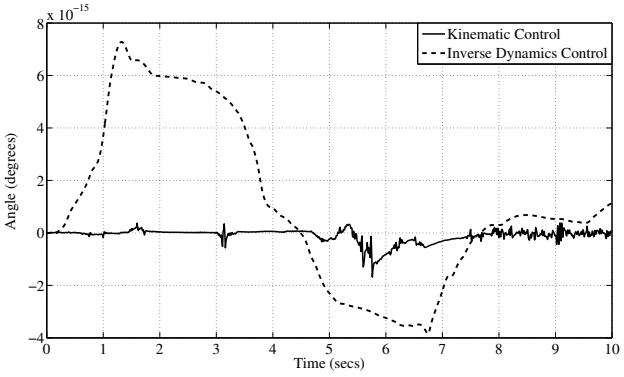

Fig. 9. UGV orientation in time for the step trajectory.

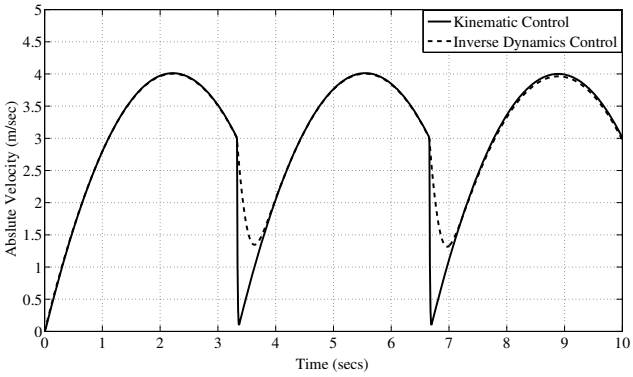

Fig. 10. Absolute velocity of UGV against time for the step trajectory.

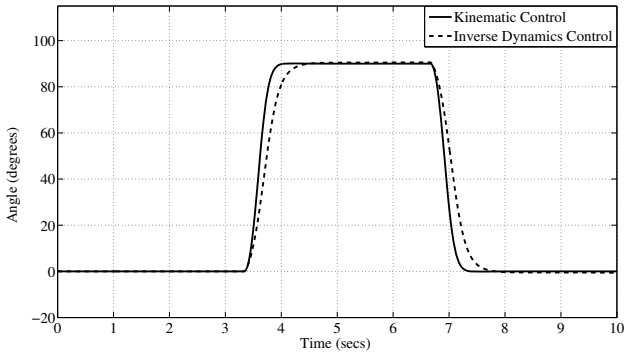

Fig. 11. Angular position of one ASOC against time for the step trajectory.

kinematic control law for the prototype vehicle. Simulation results indicate that an inverse dynamic controller performed significantly better than the kinematic controller and the UGV was able to follow the desired trajectories with good accuracy while exhibiting omnidirectional capabilities.

It is noted that the dynamic model derived in this paper is for a robot operating on a planar surface, and that it is not always appropriate to assume that outdoor terrains are planar. Thus, future work will entail experimental validation of these results in an outdoor environment. Based on the results of those experiments, a full six DOF dynamic model and controller may need to be derived and implemented.

REFERENCES

[1] S. Fish. Ugvs in future combat systems. In *SPIE Unmanned Ground Vehicle Technology VI*, pages 288–291, 2004.

[2] J. Erickson. Living the dream: an overview of the mars exploration project. *IEEE Robotics and Automation Magazine*, 13(2):12–18, 2006.

[3] J. Blitch. Artificial intelligence technologies for robot assisted urban search and rescue. *Expert Systems with Applications*, 1996.

[4] B. Yamauchi. Packbot: A versatile platform for military robotics. In *SPIE Unmanned Ground Vehicle Technology VI*, volume 5422, pages 228–237, 2004.

[5] P. Muir and C. Neuman. Kinematic modeling for feedback control of an omnidirectional wheeled mobile robot. In *IEEE International Conference on Robotics and Automation*, 1987.

[6] L. Ferriere and B. Raucent. Rollmobs, a new universal wheel concept. In *IEEE International Conference on Robotics and Automation*, pages 1877–1882, 1998.

[7] M. Wada and S. Mori. Holonomic and omnidirectional vehicle with conventional tires. In *IEEE International Conference on Robotics and Automation*, pages 3671–3676, 1996.

[8] H. Yu, S. Dubowsky, and A. Skwersky. Omni-directional mobility using active split offset casters. In *ASME Design Engineering Technical Conferences*, 2000.

[9] H. Yu, Matthew Spenko, and S. Dubowsky. Omni-directional mobility using active split offset castors. *ASME Journal of Mechanical Design*, 126(5):822–829, 2004.

[10] M. Udengaard and K. Iagnemma. Kinematic analysis and control of an omnidirectional mobile robot in rough terrain. In *Proceedings of the IEEE/RSJ International Conference on Intelligent Robots and Systems*, pages 795–800, 2007.

[11] M. Udengaard and K. Iagnemma. Design of an omnidirectional mobile robot for rough terrain. In *Proceedings of the 2008 IEEE International Conference on Robotics and Automation*, 2008.

[12] K. Iagnemma, M. Udengaard, G. Ishigami, Matthew Spenko, S. Oncu, and I. Khan. Design and development of an agile, man portable unmanned ground vehicle. In *Proceedings of the 26th Annual Army Science Conference*, 2008.

[13] Activrobots. http://www.activrobots.com/robots/seekur.html.

[14] robotmotio. http://www.robomotio.com/azimut2.php.

[15] M. Spenko, H. Yu, and S. Dubowsky. A robotic personal aid for the mobility and health monitoring of the elderly. *IEEE Transactions on Neural Systems and Rehabilitation Engineering*, 14:344–351, September 2006.

[16] Guillaume Baffet, Ali Charara, and Daniel Lechner. Estimation of vehicle sideslip, tire force and wheel cornering stiffness. *Control Engineering Practice*, In Press, Corrected Proof:–, 2009.

[17] James Lacombe. Tire model for simulations of vehicle motion on high and low friction road surfaces. In *WSC '00: Proceedings of the 32nd conference on Winter simulation*, pages 1025–1034, San Diego, CA, USA, 2000. Society for Computer Simulation International.